RSC Advances

PAPER

Cite this: *RSC Adv.*, 2016, **6**, 101911

Rational design, synthesis and 2D-QSAR studies of antiproliferative tropane-based compounds†

Nasser S. M. Ismail,*[ab] Riham F. George,[c] Rabah A. T. Serya,[b] Fady N. Baselious,[d] May El-Manawaty,[e] ElSayed M. Shalaby[f] and Adel S. Girgis*[g]

Received 26th August 2016
Accepted 5th October 2016

DOI: 10.1039/c6ra21486j

www.rsc.org/advances

3,4-Diaryl-11-methyl-7-[(aryl)methylidene]-4,5,11-triazatricyclo[6.2.1.0*2,6*]undec-5-enes **14a–s** were synthesized through reaction of 2,4-bis[(aryl)methylidene]-8-methyl-8-azabicyclo[3.2.1]octan-3-ones **12a–f** with aryl hydrazines in the presence of catalytic amount of thiamine hydrochloride. Meanwhile, the 4-acetyl analogs **16a,b** were obtained through reaction of **12b,e** and hydrazine hydrate in acetic acid. Good support for the structure was received from single crystal X-ray studies of **14a**. Some of the synthesized tropane containing-compounds showed promising antitumor properties during the *in vitro* MTT bio-assay against HepG2 (hepatocellular) and MCF7 (breast) human tumor carcinoma cell lines, with potency higher than that of doxorubicin (DNA intercalating agent, standard reference). Statistically significant 2D-QSAR model describes the antitumor properties against MCF7.

Introduction

Tropane is an important class of alkaloids found in many natural resources especially, Solanaceae, Erythroxylaceae, and Convolvulaceae plant families.[1,2] Hyoscyamine **1**, anisodamine **2** and scopolamine **3** are natural tropanes isolated from Solanaceae plants exhibiting anticholinergic properties useful for pain relief, anaesthesia, motion sickness and Parkinson's disease (Fig. 1).[3,4] *N*-Butyl hydrobromide scopolamine is useful against bladder spasms without side effects in the central nervous system. Ipratropium bromide (Atrovent®) **4** is an anticholinergic drug inhaled during asthma and tiotropium bromide (Spiriva® Boehringer Ingelheim, Pfizer) **5** is useful for chronic obstructive pulmonary disease.[5] *S*(−)Satropane **6** was approved as a stereoselective hypotensive agent on rabbit eyes due to the activation of iris muscarinic receptor.[6] Cocaine (7) is a powerful stimulant of the central nervous system capable to block the presynaptic reuptake of dopamine (DA), serotonin (5-HT) and norepinephrine (NE).[7–9] It is believed that cocaine binding to DA transporter is responsible for its reinforcing effect.[10] Cocaine abuse is a major challenge with no current effective medication however, many synthetic tropane based-analogs show promising affinity towards monoamine neurotransmitters (dopamine, serotonin, and norepinephrine) explaining the ability for application as addiction therapy development.[10–14] Recently, tropane-derived small molecules were optimized as heat shock protein 90 (HSP90) inhibitors. Inhibition of tumor cell HSP90 is an effective pathway for cancer antiproliferation.[15] Additionally, pyrazolo[1,5-*a*]pyrimidines possessing either tropane nucleus as a substituent **8** or as a fused ring system **9** were shown to be potent B-Raf inhibitors.[16] Chemotherapeutic inhibition of mutant B-Raf is an effective mean for cancer treatment.[17,18]

Inspired by all the above reports and in continuation to our program directed towards investigation of novel antitumor active agents,[19–30] it is planned in the present study to investigate synthesis of novel tropane fused pyrazoline heterocycle. Interest in the synthesis of this hybrid system is originated from the high structural resemblance to 7-arylmethylene-2,3-diaryl-3,3*a*,4,5,6,7-hexahydro-5-methyl-2*H*-pyrazolo[4,3-*c*]pyridines **10** which were reported to be promising anti-tumor active agents against a wide variety of human tumor cell lines during an *in vitro* activity screening bio-assay.[31,32] Validation of the observed biological properties is undertaken by 2D-QSAR (quantitative

[a]*Pharmaceutical Chemistry Department, Faculty of Pharmaceutical Sciences and Pharmaceutical Industries, Future University, Cairo 12311, Egypt. E-mail: saadnasser2003@yahoo.com*

[b]*Pharmaceutical Chemistry Department, Faculty of Pharmacy, Ain Shams University, Cairo, Egypt*

[c]*Pharmaceutical Chemistry Department, Faculty of Pharmacy, Cairo University, Cairo, Egypt*

[d]*Research and Development Department, Global Napi Pharmaceuticals, 6th October City, Giza, Egypt*

[e]*Pharmacognosy Department, National Research Centre, Dokki, Giza 12622, Egypt*

[f]*X-Ray Crystallography Lab., Physics Division, National Research Centre, Dokki, Giza 12622, Egypt*

[g]*Pesticide Chemistry Department, National Research Centre, Dokki, Giza 12622, Egypt. E-mail: girgisas10@yahoo.com*

† Electronic supplementary information (ESI) available: Including tables of experimental and optimized intramolecular geometrical parameters of compound **14a**, molecular descriptor values of the BMLR-QSAR model, crystal data and structure refinement parameters of compound **14a**, spectral charts of the synthesized compounds, projections of the optimized structure of compound **14a**, and dose–response curves of the tropane containing-compounds. CCDC 1499063. For ESI and crystallographic data in CIF or other electronic format see DOI: 10.1039/c6ra21486j

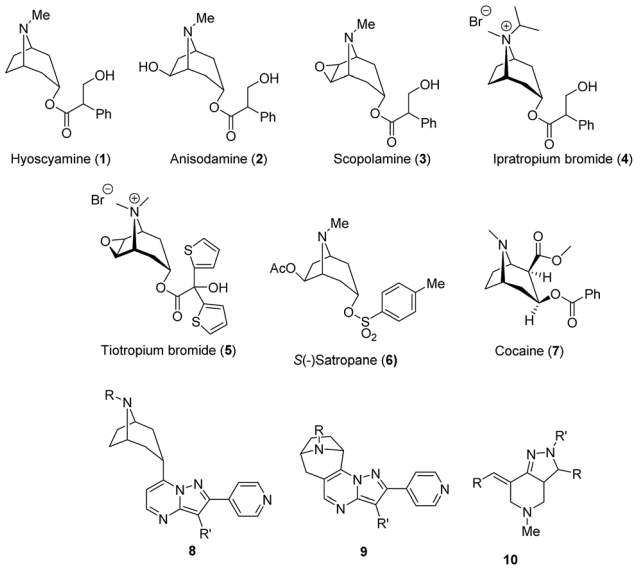

Fig. 1 Biologically active natural and synthetic tropane related-compounds.

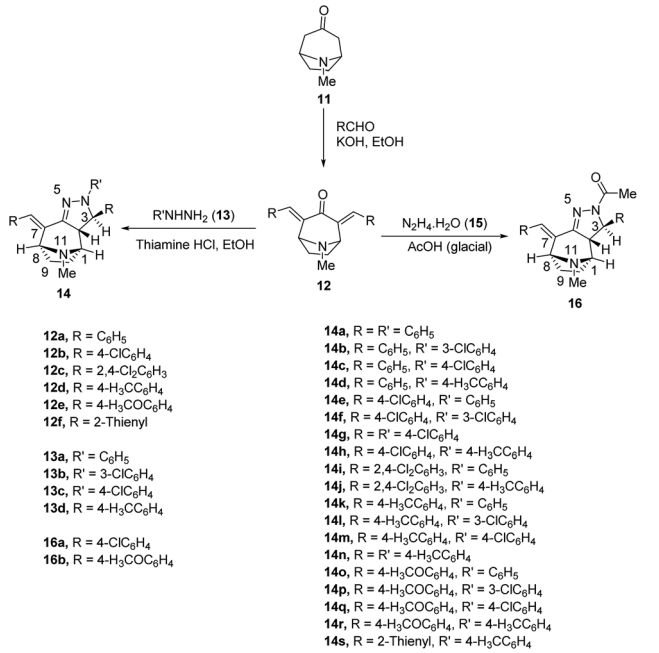

Scheme 1 Synthetic route towards tropane based-compounds.

structure–activity relationship) study which also assists in determination of the parameters controlling bio-activity. QSAR is an important tool of computer-aided drug design used intensively for developing bio-active agents and pharmacokinetics/pharmacodynamics profiling of new drugs. In QSAR the molecular structure is described mathematically in terms of physico-chemical properties "molecular descriptors". A mathematical relationship is sought between observed activity/property on one hand and molecular descriptors on the other hand. QSARs can be utilized for prediction of biological activity for compounds and/or to explain on what their biological activity depends.[33,34]

Results and discussion

Chemistry

2,4-Bis[(aryl)methylidene]-8-methyl-8-azabicyclo[3.2.1]octan-3-ones **12a–f** were synthesized through base-catalyzed condensation of 8-methyl-8-azabicyclo[3.2.1]octan-3-one **11** with aromatic aldehydes (1 : 2 molar ratio) in ethanolic potassium hydroxide solution (Scheme 1). Spectroscopic (IR, ^{1}H-, ^{13}C-NMR) and elemental analysis data support the structure of **12f**. IR spectrum of **12f** reveals the α,β-unsaturated carbonyl group (ν = 1655 cm^{-1}) as a strong stretching vibration band. The appearance of the methine olefinic protons as a sharp singlet signal at $\delta = 7.85$ supports the formation of *E*,*E*′-geometrical isomer (ESI Fig. S1–S3†).[19,22,35,36]

Reaction of 2,4-bis[(aryl)methylidene]-8-methyl-8-azabicyclo [3.2.1]octan-3-ones **12a–f** with aryl hydrazines (phenylhydrazine **13a**, 3-chlorophenyl, 4-chlorophenyl, 4-tolylhydrazine hydrochlorides **13b–d**) in refluxing ethanol in the presence of catalytic amount of thiamine hydrochloride (which is widely used as promoter for heterocyclic formation[37–41]) afforded the corresponding 3,4-diaryl-11-methyl-7-[(aryl)methylidene]-4,5,11-triazatricyclo[6.2.1.0*2,6*]undec-5-enes **14a–s** (Scheme 1). ^{1}H-NMR of **14a** (representative example of the family) shows the tropanyl methylene protons H_2C-9 and H_2C-10 as diastereotopic, coupled with each other and with the vicinal tropanyl methine protons (*HC*-8 and *HC*-1, respectively). The tropanyl H_2C-10 is appeared as a broad singlet signal ($\delta_H = 2.18$). While the upfield tropanyl H_2C-9 is shown as a multiplet signal (δ_H = 1.91–1.96) and the downfield H_2C-9 is overlapped with the tropanyl methyl protons forming broad singlet signal ($\delta_H = 2.42$).

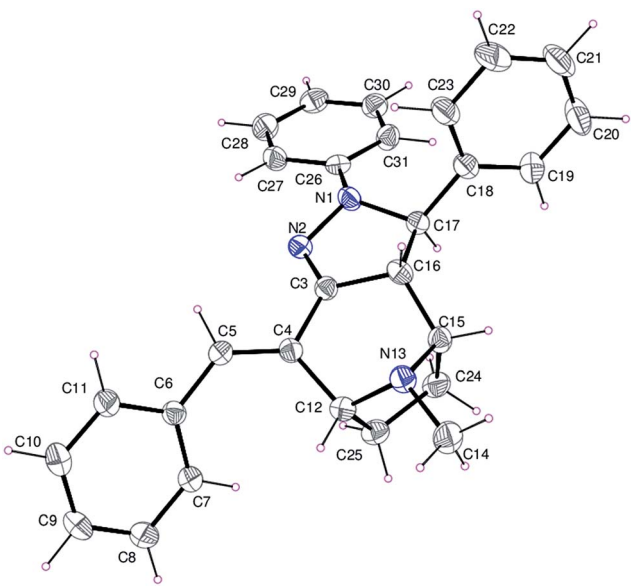

Fig. 2 An ORTEP view of compound **14a** showing the atom-numbering scheme. Displacement ellipsoids are drawn at the 30% probability level and H atoms are shown as small spheres of arbitrary radii.

The tropanyl methine protons *HC*-1 and *HC*-8 are shown as broad singlet signals at $\delta_H = 3.53$, 4.40, respectively. The pyrazolinyl *HC*-2 is appeared as double doublet signal ($\delta_H = 3.59$) and the pyrazolinyl *HC*-3 is shown as a doublet signal ($\delta_H = 4.72$) (ESI Fig. S5†). ^{1}H, ^{1}H-COSY spectrum of **14a** supports these interpretations (ESI Fig. S6†). ^{13}C-NMR spectrum of **14a** exhibits the tropanyl methylene carbons H_2C-10 and H_2C-9 at $\delta_C = 23.6$ and 30.0, respectively. The tropanyl methine carbons H*C*-8 and H*C*-1 are shown at $\delta_C = 60.9$ and 61.0, respectively. The pyrazolinyl *HC*-2 and *HC*-3 are appeared at $\delta_C = 58.4$ and 69.7, respectively (ESI Fig. S7†). ^{1}H, ^{13}C-heteronuclear single quantum coherence (HSQC) spectrum of compound **14a** supports these interpretations (ESI Fig. S8†). Single crystal X-ray diffraction of **14a** supports the structure (Fig. 2).

Reaction of 2,4-bis[(aryl)methylidene]-8-methyl-8-azabicyclo [3.2.1]octan-3-ones **12b,e** and hydrazine hydrate **15** in refluxing glacial acetic acid afforded the corresponding 4-acetyl-3-aryl-11-methyl-7-[(aryl)methylidene]-4,5,11-triazatricyclo[6.2.1.0*2,6*]-undec-5-enes **16a,b**. IR spectra of **16a,b** show the stretching vibration of acetyl carbonyl group ($\nu = 1663$, 1667 cm^{-1} for **16a**, **16b**, respectively). ^{1}H-and ^{13}C-NMR spectra of **16a,b** reveal a pattern relative to that of the synthesized **14** (ESI Fig. S1–S68† show the spectra of synthesized compounds **12f**, **14a–s** and **16a,b**).

Single crystal X-ray studies

Compound **14a** crystallizes in the orthorhombic space group $Pc2_1n$ with four molecules in the unit cell and one molecule per asymmetric unit cell. An ORTEP view of **14a** is shown in Fig. 2. The pyrazolinyl ring is sharing the C3–C16 bond with the tropanyl ring system. Two phenyl rings are attached to the pyrazolinyl ring through C18–C17 and C26–N1 bonds and another phenyl ring is connected to the tropanyl system through the exocyclic olefinic bond C4–C5. The pyrazolinyl ring exhibits an envelope configuration with the C17 atom at the flap. A similar configuration is observed for the five member azole moiety forming the tropanyl system, with the flap atom being N13. The bond lengths and angles of **14a** (ESI Tables S1 and S2†) are in good agreement with reported structures having similar molecular architecture.[42–51] The structure of compound **14a** is stabilized by a set of C–H···C and C–H···π interactions (Table 1). The C–H···C hydrogen bond creates a supramolecular assembly parallel to the (1 0 0) plane as shown in Fig. 3.

Optimized structures

The theoretical optimized bond lengths and angles of compound **14a** by different computational quantum techniques

Table 1 Hydrogen-bond geometry and non-bonding contacts (Å, °) for **14a**[a]

D–H···A	D–H	H···A	D···A	D–H···A
C22–H221···C11^{i}	0.99	2.83	3.784(4)	163.96(19)
C25–H252···Cg1^{ii}	0.98	2.84(3)	3.761(3)	158.0(2)

[a] Symmetry codes: (i) 1/2 + *x*, 1/2 + *y*, 1/2 − *z*; (ii) −1 + *x*, *y*, *z*. Cg1 = (C6, C7, C8, C9, C10, C11).

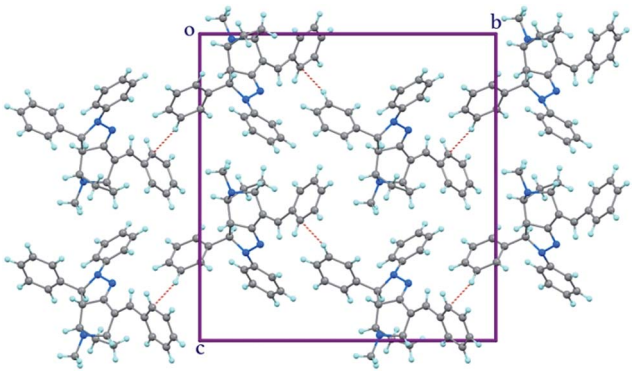

Fig. 3 A view in projection down the *a*-axis of the unit cell contents for **14a** showing supramolecular assembly parallel to the (1 0 0) plane and H-bonds as dashed lines.

AM1, PM3 and DFT (ESI Tables S1, S2 and Fig. S69–S71†) are close to the experimentally (single crystal X-ray) determined values. The minor difference values can be attributed to the crystal field and intermolecular interactions taking place between the molecules in the solid state.

The root mean square errors (RMSE) in the bond lengths are 0.0213, 0.0182 and 0.0178 while the maximum differences are 0.049, 0.045 and 0.042 Å (for AM1, PM3, and DFT methods, respectively). The RMSE of bond angles for compound **14a** are 1.97, 1.72 and 0.91, and the maximum differences are 4.8, 4.4, and 2.8° (for AM1, PM3, and DFT techniques, respectively).

Global comparisons were undertaken by superimposing the central heterocyclic skeleton (triazatricyclo[6.2.1.0*2,6*]undec-5-ene scaffold) obtained from X-ray diffraction with those of AM1, PM3 and DFT methods (ESI Fig. S72†). Most of the functional groups and attached phenyl rings are well aligned to each other with slight deviation. For structures derived from AM1 and PM3 methods, the *N*-methyl group attached to the tropanyl nitrogen is aligned nearly in opposite direction to that observed experimentally. It has also been noticed that, the phenyl ring attached to the exocyclic olefinic linkage at the tropanyl C4 and the other one attached to the pyrazolinyl N1 (numbering according to X-ray Fig. 2), have slight deviated orientations for all the optimized structures by quantum techniques utilized (AM1, PM3 and DFT) relative to the experimental X-ray structure. These observations can be attributed to the effect of the molecular packing governing the solid state, which is completely absent in the gaseous state considered for computational quantum studies.

Antitumor properties

Antitumor properties of the tropane containing-compounds **12a–f**, **14a–s** and **16a,b** were determined against HepG2 (hepatocellular) and MCF7 (breast) human tumor carcinoma cell lines utilizing the MTT standard technique.[52,53] The results (Table 2, ESI Fig. S73 and S74†) indicate that many of the tested compounds exhibit promising antitumor properties. Compounds **12a,b,d** and **14c,f,h,m,q,r** show antitumor properties against liver carcinoma (HepG2) cell line with potency

Table 2 Antitumor properties of tropane containing-compounds **12a–f**, **14a–s**, **16a,b** and doxorubicin

ID	Compd	R	R′	IC_{50}[a] (μM) HepG2	MCF7
1	**12a**	C_6H_5	—	4.9	3.4
2	**12b**	4-ClC_6H_4	—	7.2	4.0
3	**12c**	2,4-$Cl_2C_6H_3$	—	>100.0	4.4
4	**12d**	4-$H_3CC_6H_4$	—	21.7	8.3
5	**12e**	4-$H_3COC_6H_4$	—	>100.0	9.0
6	**12f**	2-Thienyl	—	66.7	14.9
7	**14a**	C_6H_5	C_6H_5	81.3	15.0
8	**14b**	C_6H_5	3-ClC_6H_4	86.6	11.3
9	**14c**	C_6H_5	4-ClC_6H_4	18.4	6.1
10	**14d**	C_6H_5	4-$H_3CC_6H_4$	48.1	9.9
11	**14e**	4-ClC_6H_4	C_6H_5	48.1	3.9
12	**14f**	4-ClC_6H_4	3-ClC_6H_4	19.0	9.3
13	**14g**	4-ClC_6H_4	4-ClC_6H_4	44.9	47.6
14	**14h**	4-ClC_6H_4	4-$H_3CC_6H_4$	11.9	5.9
15	**14i**	2,4-$Cl_2C_6H_3$	C_6H_5	>100.0	44.4
16	**14j**	2,4-$Cl_2C_6H_3$	4-$H_3CC_6H_4$	>100.0	>100.0
17	**14k**	4-$H_3CC_6H_4$	C_6H_5	92.6	5.4
18	**14l**	4-$H_3CC_6H_4$	3-ClC_6H_4	43.2	40.4
19	**14m**	4-$H_3CC_6H_4$	4-ClC_6H_4	25.0	6.8
20	**14n**	4-$H_3CC_6H_4$	4-$H_3CC_6H_4$	>100.0	21.8
21	**14o**	4-$H_3COC_6H_4$	C_6H_5	36.7	5.0
22	**14p**	4-$H_3COC_6H_4$	3-ClC_6H_4	>100.0	>100.0
23	**14q**	4-$H_3COC_6H_4$	4-ClC_6H_4	11.9	5.1
24	**14r**	4-$H_3COC_6H_4$	4-$H_3CC_6H_4$	24.2	12.1
25	**14s**	2-Thienyl	4-$H_3CC_6H_4$	>100.0	6.4
26	**16a**	4-ClC_6H_4	—	>100.0	5.5
27	**16b**	4-$H_3COC_6H_4$	—	>100.0	44.2
28	Doxorubicin	—	—	34.2	20.9

[a] IC_{50} is the concentration required to produce 50% inhibition of cell growth compared to the negative control.

higher than that of the standard reference used, doxorubicin. Meanwhile, most of the tested compounds (compounds **14g,i,j,l,n,p** and **16b** are exceptions) reveal promising antitumor properties against breast carcinoma (MCF7) cell line relative to doxorubicin. Doxorubicin is a DNA intercalating agent show broad spectrum antitumor properties against diverse variety of cancers (including leukemia, lymphoma, multiple myeloma, breast cancer, osteosarcoma, sarcoma and liver), so used intensively as a universal standard reference in antitumor studies.[54]

Through the observed antitumor data it can be concluded that, most of the tested tropane containing-compounds seem to be more effective agents against breast (MCF7) than liver (HepG2) carcinoma cell line. Compounds **12a** and **12b** exhibit considerable antitumor properties against both tested cell lines with higher potency than that of doxorubicin (IC_{50} = 4.9, 3.4; 7.2, 4.0; 34.2, 20.9 μM for **12a**, **12b** and doxorubicin against HepG2 and MCF7, respectively). Compounds **14h** and **14q** also reveal similar observations with milder potencies (IC_{50} = 11.9, 5.9; 11.9, 5.1 μM for **14h** and **14q** against HepG2 and MCF7, respectively). Meanwhile, compounds **12c**, **14e**, **14k**, **14o** and **16a** show antitumor properties against only one of the tested cell lines, MCF7 "breast carcinoma" (IC_{50} = 3.9–5.5 μM) with potency about four orders of magnitude better than the standard reference (doxorubicin, IC_{50} = 20.9 μM).

Structure–activity relationships (SAR) based on the observed antitumor properties against HepG2 (liver) carcinoma cell line, explain that insertion of a 4-chlorophenyl group at the *N*-4 of the synthesized azabicyclo[3.2.1]octans and consequently at the exocyclic olefinic linkage attached to *C*-7 enhances the antitumor properties relative to the case when the phenyl group itself is adopted as exhibited in pairs **14a**, **14c**; **14e**, **14g**; **14k**, **14m** and **14o**, **14q** (IC_{50} = 81.3, 18.4; 48.1, 44.9; 92.6, 25.0; 36.7, 11.9 μM, respectively). Additionally, 4-chlorophenyl substitution at the *N*-4 of the prepared azabicyclo[3.2.1]octans seems a better choice for developing antitumor agents compared with the 3-chlorophenyl substituent (compound **14f** is an exception) as exhibited in pairs **14b**, **14c**; **14l**, **14m** and **14p**, **14q** (IC_{50} = 86.6, 18.4; 43.2, 25.0; >100.0, 11.9 μM, respectively). It has been also noticed that, 4-methoxyphenyl substitution (IC_{50} = >100 μM for compound **12e**) brings down the potency against HepG2 about 5 fold compared with 4-methylphenyl substitution (IC_{50} = 21.7 μM for compound **12d**). This is may be due to the unfavorable electron-donating properties of functional group attached to the phenyl ring at the exocyclic olefinic linkage, which is also supported by the enhanced property for compound **12b** bearing 4-chlorophenyl substitution (IC_{50} = 7.2 μM).

SAR concluded from the observed antitumor properties against MCF7 (breast) carcinoma cell line shows also controlling parameters similar to those of HepG2. Utilization of a 4-chlorophenyl group at the *N*-4 of the synthesized azabicyclo [3.2.1]octans enhances the observed bio-properties relative to the 3-chlorophenyl moiety (**14g** is an exception) as exhibited in pairs **14b**, **14c**; **14l**, **14m** and **14p**, **14q** (IC_{50} = 11.3, 6.1; 40.4, 6.8; >100.0, 5.1 μM, respectively). 4-Chlorophenyl substitution at the *N*-4 seems also a better choice for developing bio-active agents compared with the 4-methylphenyl group (**14g** is an exception) as exhibited in pairs **14c**, **14d**; **14m**, **14n** and **14q**, **14r** (IC_{50} = 6.1, 9.9; 6.8, 21.8; 5.1, 12.1 μM, respectively). It has been also noticed that, 3-chlorophenyl substitution at *N*-4 (compound **14b** is an exception) reduces drastically the antitumor potency relative to the phenyl group itself as exhibited in pairs **14e**, **14f**; **14k**, **14l** and **14o**, **14p** (IC_{50} = 3,9, 9.3; 5.4, 40.4; 5.0, >100.0 μM for compounds **14e**, **14f**; **14k**, **14l** and **14o**, **14p**, respectively). For better understanding the observed pharmacological properties and determine the structural parameters controlling bio-activities, 2D-QSAR studies were undertaken.

2D-QSAR studies

2D-QSAR studies were undertaken utilizing CODESSA-Pro (comprehensive descriptors for structural and statistical analysis) software employing 25 bio-active tropane containing-compounds (**12a–f**, **14a–i,k–o,q–s** and **16a,b**) which exhibit variable antitumor properties against MCF7 (breast) carcinoma cell line. The best multi-linear regression QSAR (BMLR-QSAR) model obtained for the present study is statistically significant. The 5 descriptors controlling the QSAR model are presented in Table 3. Fig. 4 shows the BMLR-QSAR model plot of correlations representing the observed *versus* predicted IC_{50},

Table 3 Descriptor of the BMLR-QSAR model for the antitumor tropane containing-compounds (**12a–f**, **14a–i,k–o,q–s** and **16a,b**) against MCF7 (beast) carcinoma cell line[a]

Entry	ID	Coefficient	*s*	*t*	Descriptor
1	0	−130.182	24.798	−5.250	Intercept
2	D_1	0.039	0.004	9.510	Shadow plane *YZ*
3	D_2	21.035	3.486	6.033	Max. bond order for atom C
4	D_3	0.344	0.059	5.798	Min. (#HA, #HD) (Zefirov PC)
5	D_4	2.284	0.590	3.868	Min. n–n repulsion for bond H–C
6	D_5	−0.214	0.032	−6.613	Square root of surface area for atom N

[a] $N = 25$, $n = 5$, $R^2 = 0.857$, $R^2\text{cvOO} = 0.767$, $R^2\text{cvMO} = 0.774$, $F = 22.715$, $s^2 = 0.023$. $\log(\text{IC}_{50}) = -130.182 + (0.039 \times D_1) + (21.035 \times D_2) + (0.344 \times D_3) + (2.284 \times D_4) - (0.214 \times D_5)$.

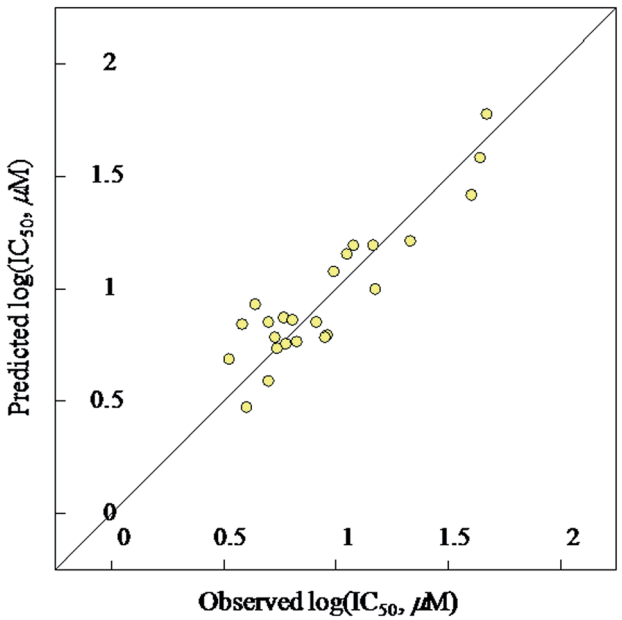

Fig. 4 BMLR-QSAR model plot of correlations representing the observed *versus* predicted log(IC_{50}, μM) values for the tropane containing-compounds (**12a–f**, **14a–i,k–o,q–s** and **16a,b**) against MCF7 (beast) carcinoma cell line.

Table 4 Observed and estimated/predicted activity values for the antitumor tropane containing-compounds (**12a–f**, **14a–i,k–o,q–s** and **16a,b**) according to the BMLR-QSAR model due to MCF7 (breast) carcinoma cell line

Entry	Compd	Observed IC_{50}, μM	Estimated IC_{50}, μM	Error[a]
1	**12a**	3.4	4.8	−1.4
2	**12b**	4.0	3.0	1.0
3	**12c**	4.4	8.4	−4.0
4	**12d**	8.3	7.1	1.2
5	**12e**	9.0	6.1	2.9
6	**12f**	14.9	15.6	−0.7
7	**14a**	15.0	9.8	5.2
8	**14b**	11.3	14.0	−2.7
9	**14c**	6.1	5.6	0.5
10	**14d**	9.9	11.9	−2.0
11	**14e**	3.9	6.9	−3.0
12	**14f**	9.3	6.2	3.1
13	**14g**	47.6	59.0	−11.4
14	**14h**	5.9	7.4	−1.5
15	**14i**	44.4	37.8	6.6
16	**14k**	5.4	6.0	−0.6
17	**14l**	40.4	26.2	14.2
18	**14m**	6.8	5.7	1.1
19	**14n**	21.8	16.2	5.6
20	**14o**	5.0	3.9	1.1
21	**14q**	5.1	7.0	−1.9
22	**14r**	12.1	15.5	−3.4
23	**14s**	6.4	7.3	−0.9
24	**16a**	5.5	5.4	0.1
25	**16b**	44.2	38.0	6.2

[a] Error is the difference between the observed and estimated bio-activity values.

μM values for the bio-active tropane containing-compounds. The plots are uniformly scattered [observed 0.531–1.678, predicted 0.472–1.771; log(IC_{50}, μM)]. Table 4 reveals the observed and estimated/predicted IC_{50} (μM) values of the antitumor active training set tropane containing-compounds.

Shadow plane *YZ* is the first descriptor controlling the MCF7-QSAR model ($t = 9.510$). It is a geometrical descriptor reflecting the molecular size and participates positively in the QSAR model. Lower descriptor value reflects higher potency of the molecule, considering the intercept of the BMLR-QSAR with negative sign (−130.182) (descriptor values of the 2D-QSAR model are presented in ESI Table S3†). Maximum bond order for atom C is a semi-empirical descriptor describing the unsaturation and aromaticity of the molecule. Although this descriptor has the highest coefficient value among all QSAR model's descriptors (coefficient = 21.035), its effect on the training set analogs' potencies is so minor. This is due to the chemical structure resemblance of the training set compounds (same scaffold/ring system). Minimum (#HA, #HD) (Zefirov PC) is a charge-related descriptor. Appearance of this descriptor as an important controlling parameter governing bio-properties correlates well with the SAR observations exhibiting the importance of the electron donating/withdrawing groups of the phenyl ring attached to the *N*-4 of the synthesized triazatricyclo [6.2.1.0*2,6*]undec-5-enes. Hydrogen bonding acceptor/donor ability of the molecule (HACA1, HDSA1) is determined by eqn (1) and (2).[55]

$$\text{HACA1} = \sum_A S_A,\ A \in X_{\text{H-acceptor}} \quad (1)$$

where, S_A is solvent-accessible surface area of H-bonding acceptor atoms, selected by threshold charge.

$$\mathrm{HDSA1} = \sum_D S_D,\ D \in H_{\text{H-donor}} \quad (2)$$

where, S_D is solvent-accessible surface area of H-bonding donor H atoms.

Minimum n–n repulsion for bond H–C is a semi-empirical descriptor. Electron–electron repulsion between two given atoms is determined by eqn (3).[55]

$$E_{ee}(AB) = \sum_{\mu,\nu\in A}\sum_{\lambda,\sigma\in B} P_{\mu\nu}P_{\lambda\sigma}\langle\mu\nu|\lambda\sigma\rangle \quad (3)$$

where, A is a given atomic species, B is another atomic species, $P_{\mu\nu}P_{\lambda\sigma}$ is the density matrix elements over atomic basis $\{\mu\nu\lambda\sigma\}$, $\langle\mu\nu|\lambda\sigma\rangle$ is the electron repulsion integrals on atomic basis $\{\mu\nu\lambda\sigma\}$.

Square root of surface area for atom N is a charge-related descriptor. The partial positively charged surface area is determined by eqn (4).[55]

$$\mathrm{PPSA1} = \sum_A S_A,\ A \in \{\delta_A > 0\} \quad (4)$$

where, S_A is the positively charged solvent-accessible atomic surface area.

Due to the limited data set utilized (25 tropane containing-compounds) and absence of biologically active external data points against MCF7 cell line with the same chemical scaffold useful for the present QSAR study, internal validation technique is mainly considered to be the most appropriate.[24,56–59] CODESSA-Pro has the power for determining R^2cvOO (squared cross-validation correlation coefficient with leave one out "one example omitted at a time" = 0.767) and R^2cvMO (squared cross-validation correlation coefficient with leave many out "many data points omitted at a time up to 20% of the total data points" = 0.774), which are close to the squared correlation coefficient of the BMLR-QSAR model (R^2 = 0.857). Standard deviation of the regression (s^2 = 0.023) relative to Fisher test value (F = 22.715) also statistical parameters support the robustness of the 2D-QSAR model.

The predicted IC_{50} values for the high potent antitumor active tropane containing compounds against MCF7 cell line **12a–e**, **14c–f,h,k,m,o,q,s** and **16a** (3.0–11.9 μM) are correlated with the observed bio-properties ($IC_{50(observed)}$ = 3.4–9.9 μM) exhibiting acceptable error values = 0.1–4.0. Compounds **12f** and **14a,b,r** which are also with good antitumor potency ($IC_{50(observed)}$ = 11.3–15.0 μM) relative to the reference standard, doxorubicin (IC_{50} = 20.9 μM) show comparable predicted bio-data ($IC_{50(predicted)}$ = 9.8–15.6 μM) with error value range = 0.7–5.2. Meanwhile, compounds **14g,i,l** and **16b**, which are low antitumor effective agents against MCF7 ($IC_{50(observed)}$ = 40.4–47.6 μM) exhibit predicted properties ($IC_{50(predicted)}$ = 26.2–59.0 μM) with relatively higher error values (6.2–14.2) (Table 4). From all the above observations, it can be concluded that the attained 2D-QSAR model is applicable not only for the high potent antitumor hits against MCF7 cell line but also for the low effective agents.

Table 5 ADMET descriptor values for the antitumor active agents against MCF7 cell line

ID	Compd	Aqueous solubility[a]	Intestinal absorption[b]	BBB[c]	PPB[d]	Hepatotoxicity[e]
1	**12a**	2	0	0	2	1
2	**12b**	1	1	0	2	1
3	**12c**	0	3	4	2	1
4	**12d**	1	0	0	2	1
5	**12e**	2	0	1	2	1
6	**12f**	2	0	0	2	1
7	**14a**	1	1	0	2	1
8	**14b**	0	1	0	2	1
9	**14c**	0	1	0	2	1
10	**14d**	1	1	0	2	0
11	**14e**	0	3	4	2	1
12	**14f**	0	3	4	2	1
13	**14g**	0	3	4	2	1
14	**14h**	0	3	4	2	0
15	**14i**	0	3	4	2	1
16	**14k**	0	2	0	2	1
17	**14l**	0	3	4	2	1
18	**14m**	0	3	4	2	0
19	**14n**	0	3	4	2	0
20	**14o**	1	0	0	2	1
21	**14q**	1	1	0	2	1
22	**14r**	1	1	0	2	1
23	**14s**	1	1	0	2	1
24	**16a**	1	0	0	2	1
25	**16b**	2	0	1	2	1

[a] Aqueous solubility level: 0, extremely low; 1, very low; 2, low; 3, good; 4, optimal; 5, too soluble; 6, unknown. [b] Intestinal absorption level: 0, good; 1, moderate; 2, poor; 3 very poor. [c] Blood brain barrier penetration (BBB) level: 0, very good; 1, high; 2, medium; 3, low; 4, very low. [d] Plasma protein binding (PPB) level: 0, <90%; 1, >90%; 2, >95%. [e] Hepatotoxicity level: 0, non toxic; 1, toxic.

In order to attain appropriate validation of the QSAR study, part of the available data set was utilized for building the model and the remaining data points were used as an external test set (external validation).[60,61] From the observed results (ESI Tables S4–S12 and Fig. S75–S77†) it has been noticed that, 3 descriptor ($n = 3$) statistically significant BMLR-QSAR models ($N = 16$–17) are obtained due to this validation technique ($R^2 = 0.711$, 0.768, 0.790 for the subset groups $A + B$, $A + C$ and $B + C$, respectively). Additionally, the estimated/predicted properties for most of the test set compounds are correlated with their experimental observed activities preserving their potencies among each other.

ADMET studies

ADMET (absorption, distribution, metabolism, excretion, toxicity) studies of the antitumor active agents against MCF7 cell line were undertaken by Discovery Studio 2.5 software (http://accelrys.com/products/collaborative-science/biovia-discovery-studio/). The ADMET descriptor values are presented in Table 5. From the results obtained it has been noticed that, compounds **12a,e,f**; **16b** exhibit low aqueous solubility level (2) however, the remaining analogs are either extremely low (0) or very low (1). This is obvious due to the aromatic properties of the synthesized tropanes. Compounds **12a,d–f**; **14o**, **16a,b** reveal good intestinal absorption level (0). However, compounds **12b**; **14a–d,q–s** show moderate intestinal absorption level (1). Compounds **12a,b,d,f**; **14a–d,k,o,q–s**; **16a** show very good blood brain barrier (BBB) penetration level (0) and all the tested compounds (**12a–f**, **14a–i,k–o,q–s** and **16a,b**) exhibit plasma protein binding (PPB) level >95%. The PPB predicts whether a compound is bound to carrier proteins in the blood. From the observed results, there is high probability that many of the synthesized tropanes can reach the desired targets.

Conclusions

In conclusion, antitumor active tropane containing-compounds **14a–s** and **16a,b** are readily synthesized in fair to good yields (50–85%) through reaction of 2,4-bis[(aryl)methylidene]-8-methyl-8-azabicyclo[3.2.1]octan-3-ones **12a–f** with hydrazines. Some of the synthesized tropane containing-compounds **14** and **16** in addition to the starting agents **12** reveal promising antitumor properties through *in vitro* MTT standard technique against HepG2 (hepatocellular) and MCF7 (breast) cancer cell lines with potency higher than doxorubicin (standard reference). Statistically significant 2D-QSAR with 5 descriptors model describes the antitumor properties against MCF7. Although short data set is used in the QSAR study, homogeneity of the set (same chemical scaffold) may be the main factor contributing the success of the computational study that can be used for further optimization of effective antitumor hits.

Experimental section

Chemistry

Melting points were recorded on a Stuart SMP10 melting point apparatus. IR spectra (KBr) were recorded on a Shimadzu FT-IR 8400S spectrophotometer. NMR spectra ($CDCl_3$) were recorded on a Bruker Ascend 400/R (^{1}H: 400 MHz ^{13}C: 100 MHz) spectrometer. Elemental analyses were determined by the Regional Center for Mycology and Biotechnology, Al-Azhar University, Egypt, utilizing FLASH 2000 CHNS/O analyzer, Thermo Scientific. Compounds **12a–e**[62,63] were prepared according to the reported procedures.

Synthesis of 2,4-bis[(2-thienyl)methylidene]-8-methyl-8-azabicyclo[3.2.1]octan-3-one (12f). A mixture of 8-methyl-8-azabicyclo[3.2.1]octan-3-one **11** (5 mmol) and 2-thiophenecarbaldehyde (0.94 ml, 10 mmol) in absolute ethanol (25 ml) containing potassium hydroxide (10 mmol), was stirred at room temperature (25 °C) overnight. The separated solid was collected, washed with water and crystallized from ethanol affording **12f** as buff microcrystals, mp 167–169 °C, yield 69% (1.12 g). IR ν (cm^{-1}): 1655, 1589, 1566. ^{1}H-NMR δ (ppm): 1.76 (sextet, $J = 2.4$, 6.3, 13.8 Hz, 2H), 2.36 (s, 3H), 2.54 (quintet, $J = 2.7$, 7.1, 11.4 Hz, 2H), 4.60 (dd, $J = 2.5$, 4.4 Hz, 2H), 7.07 (dd, $J = 3.7$, 5.1 Hz, 2H), 7.25 (d, $J = 3.6$ Hz, 2H), 7.45 (d, $J = 5.1$ Hz, 2H), 7.85 (s, 2H). ^{13}C-NMR δ (ppm): 29.8, 36.2, 61.3, 128.0, 128.9, 130.1, 133.2, 135.6, 138.3, 186.6. Elemental analysis: $C_{18}H_{17}NOS_2$ required C, 66.02; H, 5.23; N, 4.28, found C, 66.19; H, 5.31; N, 4.39.

Synthesis of 3,4-diaryl-11-methyl-7-[(aryl)methylidene]-4,5,11-triazatricyclo[6.2.1.0*2,6*]undec-5-enes 14a–s (general procedure). A mixture of equimolar amounts of the appropriate 2,4-bis[(aryl)methylidene]-8-methyl-8-azabicyclo[3.2.1]octan-3-ones **12a–f** and aryl hydrazine (phenylhydrazine **13a**, 3-chlorophenyl, 4-chlorophenyl, 4-tolylhydrazine hydrochlorides **13b–d**) (5 mmol) in absolute ethanol (25 ml) containing catalytic amount of thiamine hydrochloride (100 mg) was boiled under reflux for the appropriate time (TLC control). The formed solid upon cooling the reaction mixture till room temperature was collected and crystallized from a suitable solvent affording the corresponding **14a,e,i,k,o**. In case of **14b–d,f–h,j,l–n,p–s**, the reaction mixture was poured into ice-cold water (200 ml) and neutralized (sodium hydroxide, 5 N). The isolated sticky mass was triturated with ethanol (5–10 ml) and the separated solid was collected and crystallized from a suitable solvent affording the corresponding analogs.

*3,4-Diphenyl-11-methyl-7-[(phenyl)methylidene]-4,5,11-triazatricyclo[6.2.1.0*2,6*]undec-5-ene (**14a**).* Obtained from reaction of **12a** and **13a**. Reaction time 6 h, pale yellow microcrystals from ethanol, mp 201–203 °C, yield 62% (1.25 g). IR ν (cm^{-1}): 1597, 1570, 1497. ^{1}H-NMR δ (ppm): 1.91–1.96 (m, 1H), 2.18 (br s, 2H), 2.42 (br s, 4H), 3.53 (br s, 1H), 3.59 (dd, $J = 3.9$, 13.0 Hz, 1H), 4.40 (br s, 1H), 4.72 (d, $J = 12.8$ Hz, 1H), 6.87 (t, $J = 7.2$ Hz, 1H), 7.08 (d, $J = 8.5$ Hz, 2H), 7.20 (t, $J = 8.0$ Hz, 2H), 7.27–7.42 (m, 11H). ^{13}C-NMR δ (ppm): 23.6, 30.0, 36.5, 58.4, 60.9, 61.0, 69.7, 115.1, 120.3, 125.3, 126.1, 127.4, 127.8, 128.4, 128.8, 129.3, 129.5, 133.4, 136.0, 141.7, 146.6, 150.1. Elemental analysis: $C_{28}H_{27}N_3$ required C, 82.93; H, 6.71; N, 10.36, found C, 83.14; H, 6.76; N, 10.54.

*4-(3-Chlorophenyl)-11-methyl-3-phenyl-7-[(phenyl)methylidene]-4,5,11-triazatricyclo[6.2.1.0*2,6*]undec-5-ene (**14b**).* Obtained from reaction of **12a** and **13b**. Reaction time 6 h, pale yellow microcrystals from ethanol, mp 181–183 °C, yield 66% (1.45 g).

IR ν (cm^{-1}): 1593, 1566, 1481. ^{1}H-NMR δ (ppm): 1.88–1.94 (m, 1H), 2.08–2.17 (m, 2H), 2.37–2.43 (m, 4H), 3.47 (t, J = 5.2 Hz, 1H), 3.59 (dd, J = 4.2, 12.6 Hz, 1H), 4.31 (d, J = 6.9 Hz, 1H), 4.67 (d, J = 12.6 Hz, 1H), 6.77–6.83 (m, 2H), 7.06 (t, J = 8.1 Hz, 1H), 7.22 (t, J = 1.8 Hz, 1H), 7.24 (s, 1H), 7.28–7.36 (m, 3H), 7.39–7.45 (m, 7H). ^{13}C-NMR δ (ppm): 23.7, 30.1, 36.6, 58.9, 60.97, 61.0, 69.5, 112.6, 115.4, 120.0, 125.4, 126.0, 127.5, 128.0, 128.4, 129.4, 129.5, 129.7, 133.6, 134.6, 135.9, 141.3, 147.7, 151.1. Elemental analysis: $C_{28}H_{26}ClN_3$ required C, 76.44; H, 5.96; N, 9.55, found C, 76.78; H, 6.11; N, 9.78.

*4-(4-Chlorophenyl)-11-methyl-3-phenyl-7-[(phenyl)methylidene]-4,5,11-triazatricyclo[6.2.1.0*2,6*]undec-5-ene* ***(14c)****.* Obtained from reaction of **12a** and **13c**. Reaction time 12 h, pale yellow microcrystals from ethanol, mp 212–214 °C, yield 68% (1.50 g). IR ν (cm^{-1}): 1593, 1560, 1489. ^{1}H-NMR δ (ppm): 1.89–1.96 (m, 1H), 2.10–2.23 (m, 2H), 2.40 (s, 3H), 2.42–2.47 (m, 1H), 3.49 (t, J = 5.1 Hz, 1H), 3.59 (dd, J = 4.2, 12.8 Hz, 1H), 4.33 (d, J = 6.9 Hz, 1H), 4.66 (d, J = 12.8 Hz, 1H), 6.99 (d, J = 9.0 Hz, 2H), 7.13 (d, J = 9.0 Hz, 2H), 7.25 (s, 1H), 7.29–7.44 (m, 10H). ^{13}C-NMR δ (ppm): 23.6, 30.0, 36.4, 58.5, 61.0, 69.7, 116.3, 125.2, 125.7, 126.0, 127.6, 128.0, 128.5, 128.7, 129.4, 133.0, 135.8, 141.1, 145.1, 150.4. Elemental analysis: $C_{28}H_{26}ClN_3$ required C, 76.44; H, 5.96; N, 9.55, found C, 76.61; H, 6.04; N, 9.71.

*11-Methyl-4-(4-methylphenyl)-3-phenyl-7-[(phenyl)methylidene]-4,5,11-triazatricyclo[6.2.1.0*2,6*]undec-5-ene* ***(14d)****.* Obtained from reaction of **12a** and **13d**. Reaction time 5 h, pale yellow microcrystals from ethanol, mp 190–192 °C, yield 74% (1.55 g). IR ν (cm^{-1}): 1612, 1540, 1512. ^{1}H-NMR δ (ppm): 1.88–1.95 (m, 1H), 2.14–2.19 (m, 2H), 2.27 (s, 3H), 2.37–2.46 (m, 4H), 3.47 (dd, J = 4.1, 7.5 Hz, 1H), 3.59 (dd, J = 4.3, 13.0 Hz, 1H), 4.31 (d, J = 6.9 Hz, 1H), 4.68 (d, J = 13.0 Hz, 1H), 7.01 (t, J = 9.6 Hz, 4H), 7.25 (s, 1H), 7.28–7.37 (m, 4H), 7.39–7.45 (m, 6H). ^{13}C-NMR δ (ppm): 20.5, 23.7, 30.1, 36.6, 58.5, 60.87, 60.9, 70.1, 115.3, 124.7, 126.2, 127.3, 127.7, 128.3, 129.2, 129.3, 129.5, 129.6, 134.0, 136.2, 141.9, 144.6, 150.2. Elemental analysis: $C_{29}H_{29}N_3$ required C, 83.02; H, 6.97; N, 10.02, found C, 83.17; H, 7.04; N, 10.23.

*3-(4-Chlorophenyl)-7-[(4-chlorophenyl)methylidene]-11-methyl-4-phenyl-4,5,11-triazatricyclo[6.2.1.0*2,6*]undec-5-ene* ***(14e)****.* Obtained from reaction of **12b** and **13a**. Reaction time 6 h, pale yellow microcrystals from ethanol, mp 201–203 °C, yield 55% (1.3 g). IR ν (cm^{-1}): 1597, 1566, 1501, 1489. ^{1}H-NMR δ (ppm): 1.86–1.92 (m, 1H), 2.09–2.19 (m, 2H), 2.41–2.44 (m, 4H), 3.48 (br s, 1H), 3.53 (dd, J = 3.9, 12.9 Hz, 1H), 4.26 (d, J = 5.0 Hz, 1H), 4.68 (d, J = 12.8 Hz, 1H), 6.89 (t, J = 7.3 Hz, 1H), 7.03 (d, J = 8.4 Hz, 2H), 7.18–7.23 (m, 5H), 7.34–7.40 (m, 7H). ^{13}C-NMR δ (ppm): 23.6, 29.9, 36.7, 58.6, 60.9, 60.93, 69.0, 115.1, 120.6, 123.8, 127.5, 128.6, 128.8, 129.5, 130.7, 133.3, 133.5, 134.3, 134.4, 140.2, 146.3, 150.1. Elemental analysis: $C_{28}H_{25}Cl_2N_3$ required C, 70.89; H, 5.31; N, 8.86, found C, 71.14; H, 5.34; N, 8.98.

*3-(4-Chlorophenyl)-4-(3-chlorophenyl)-7-[(4-chlorophenyl)methylidene]-11-methyl-4,5,11-triazatricyclo[6.2.1.0*2,6*]undec-5-ene* ***(14f)****.* Obtained from reaction of **12b** and **13b**. Reaction time 8 h, pale yellow microcrystals from ethanol, mp 232–234 °C, yield 51% (1.3 g). IR ν (cm^{-1}): 1593, 1570, 1481. ^{1}H-NMR δ (ppm): 1.85–1.91 (m, 1H), 2.04–2.22 (m, 2H), 2.37–2.46 (m, 4H), 3.46 (t, J = 5.3 Hz, 1H), 3.53 (dd, J = 4.0, 12.6 Hz, 1H), 4.24 (d, J = 6.9 Hz, 1H), 4.64 (d, J = 12.5, 1H), 6.73 (dd, J = 1.6, 8.3 Hz, 1H), 6.84 (dd, J = 1.2, 7.9 Hz, 1H), 7.07 (t, J = 8.1 Hz, 1H), 7.16–7.23 (m, 4H), 7.32–7.41 (m, 6H). ^{13}C-NMR δ (ppm): 23.6, 30.0, 36.8, 59.0, 61.0, 68.8, 112.6, 115.4, 120.3, 124.1, 127.3, 128.7, 129.7, 129.8, 130.7, 133.4, 133.7, 134.2, 134.3, 134.7, 139.8, 147.3, 151.0. Elemental analysis: $C_{28}H_{24}Cl_3N_3$ required C, 66.09; H, 4.75; N, 8.26, found C, 66.35; H, 4.83; N; 8.38.

*3,4-Bis(4-chlorophenyl)-7-[(4-chlorophenyl)methylidene]-11-methyl-4,5,11-triazatricyclo[6.2.1.0*2,6*]undec-5-ene* ***(14g)****.* Obtained from reaction of **12b** and **13c**. Reaction time 12 h, almost colorless microcrystals from ethanol, mp 220–222 °C, yield 53% (1.35 g). IR ν (cm^{-1}): 1593, 1558, 1489. ^{1}H-NMR δ (ppm): 1.88–1.94 (m, 1H), 2.09–2.23 (m, 2H), 2.43–2.47 (m, 4H), 3.52–3.56 (m, 2H), 4.29 (d, J = 6.1 Hz, 1H), 4.64 (d, J = 12.5 Hz, 1H), 6.92–6.96 (m, 2H), 7.12–7.22 (m, 5H), 7.31–7.41 (m, 6H). ^{13}C-NMR δ (ppm): 23.6, 29.9, 36.7, 58.8, 60.9, 69.1, 116.2, 124.1, 125.5, 127.4, 128.67, 128.7, 129.6, 130.6, 133.4, 133.8, 134.0, 134.3, 139.7, 144.8, 150.5. Elemental analysis: $C_{28}H_{24}Cl_3N_3$ required C, 66.09; H, 4.75; N, 8.26, found C, 66.38; H, 4.79; N, 8.42.

*3-(4-Chlorophenyl)-7-[(4-chlorophenyl)methylidene]-4-(4-methylphenyl)-11-methyl-4,5,11-triazatricyclo[6.2.1.0*2,6*]undec-5-ene* ***(14h)****.* Obtained from reaction of **12b** and **13d**. Reaction time 8 h, pale yellow microcrystals from ethanol, mp 206–208 °C, yield 51% (1.25 g). IR ν (cm^{-1}): 1609, 1555, 1508, 1489. ^{1}H-NMR δ (ppm): 1.88–1.91 (m, 1H), 2.11–2.19 (m, 2H), 2.26 (s, 3H), 2.41–2.45 (m, 4H), 3.47–3.53 (m, 2H), 4.26 (d, J = 6.5 Hz, 1H), 4.64 (d, J = 12.8 Hz, 1H), 6.93 (d, J = 8.6 Hz, 2H), 7.01 (d, J = 8.4 Hz, 2H), 7.17 (s, 1H), 7.21 (d, J = 8.4 Hz, 2H), 7.32–7.39 (m, 6H). ^{13}C-NMR δ (ppm): 20.5, 23.6, 29.9, 36.8, 58.5, 60.9, 69.4, 115.3, 123.5, 127.5, 128.6, 129.4, 129.5, 130.0, 130.7, 133.2, 133.4, 134.5, 134.52, 140.3, 144.2, 149.9. Elemental analysis: $C_{29}H_{27}Cl_2N_3$ required C, 71.31; H, 5.57; N, 8.60, found C, 71.49; H, 5.62; N, 8.67.

*3-(2,4-Dichlorophenyl)-7-[(2,4-dichlorophenyl)methylidene]-11-methyl-4-phenyl-4,5,11-triazatricyclo[6.2.1.0*2,6*]undec-5-ene* ***(14i)****.* Obtained from reaction of **12c** and **13a**. Reaction time 6 h, pale yellow microcrystals from *n*-butanol, mp 220–222 °C (lit. mp 220–222 °C (ref. 63)), yield 85% (2.3 g). IR ν (cm^{-1}): 1597, 1574, 1497, 1466. ^{1}H-NMR δ (ppm): 1.78–1.85 (m, 1H), 2.09–2.14 (m, 2H), 2.27–2.34 (m, 4H), 3.48 (dd, J = 4.2, 12.5 Hz, 1H), 3.62–3.63 (m, 1H), 3.93 (d, J = 6.9 Hz, 1H), 5.17 (d, J = 12.6 Hz, 1H), 6.85–7.50 (m, 12H). ^{13}C-NMR δ (ppm): 23.7, 29.9, 36.5, 58.4, 61.1, 61.5, 65.4, 114.9, 115.3, 120.8, 126.8, 128.5, 129.0, 129.1, 129.6, 131.5, 132.5, 132.8, 133.9, 134.0, 135.3, 135.6, 137.6, 145.6. Elemental analysis: $C_{28}H_{23}Cl_4N_3$ required C, 61.90; H, 4.27; N, 7.73, found C, 62.04; H, 4.29; N, 7.81.

*3-(2,4-Dichlorophenyl)-7-[(2,4-dichlorophenyl)methylidene]-4-(4-methylphenyl)-11-methyl-4,5,11-triazatricyclo[6.2.1.0*2,6*]undec-5-ene* ***(14j)****.* Obtained from reaction of **12c** and **13d**. Reaction time 6 h, pale yellow microcrystals from ethanol, mp 233–235 °C, yield 65% (1.8 g). IR ν (cm^{-1}): 1612, 1512, 1470. ^{1}H-NMR δ (ppm): 1.87–1.92 (m, 1H), 2.20–2.27 (m, 5H), 2.41 (br s, 4H), 3.53 (d, J = 9.6 Hz, 1H), 3.71 (br s, 1H), 4.02 (d, J = 4.7 Hz, 1H), 5.20 (d, J = 12.7 Hz, 1H), 6.87 (d, J = 8.6 Hz, 2H), 7.03 (d, J = 8.3 Hz, 2H), 7.11 (d, J = 8.2 Hz, 1H),

7.17 (s, 1H), 7.25–7.27 (m, 2H), 7.48 (dd, J = 2.1, 3.7 Hz, 2H), 7.57 (d, J = 8.4 Hz, 1H). ^{13}C-NMR δ (ppm): 20.5, 23.7, 29.8, 36.5, 58.1, 61.1, 61.5, 65.7, 115.0, 126.8, 128.5, 129.2, 129.5, 129.59, 129.61, 130.3, 131.5, 132.5, 132.8, 133.9, 134.0, 135.3, 137.6, 143.5, 148.7. Elemental analysis: $C_{29}H_{25}Cl_4N_3$ required C, 62.50; H, 4.52; N, 7.54, found C, 62.78; H, 4.47; N, 7.68.

*11-Methyl-3-(4-methylphenyl)-7-[(4-methylphenyl)methylidene]-4-phenyl-4,5,11-triazatricyclo[6.2.1.0*2,6*]undec-5-ene (**14k**).* Obtained from reaction of **12d** and **13a**. Reaction time 4 h, pale yellow microcrystals from ethanol, mp 209–211 °C, yield 67% (1.45 g). IR ν (cm^{-1}): 1597, 1566, 1497. ^{1}H-NMR δ (ppm): 1.94–1.97 (m, 1H), 2.20–2.24 (m, 2H), 2.39 (s, 3H), 2.40 (s, 3H), 2.45 (br s, 4H), 3.57 (br d, J = 10.4 Hz, 2H), 4.40 (br s, 1H), 4.69 (d, J = 13.0 Hz, 1H), 6.87 (t, J = 7.2 Hz, 1H), 7.08 (d, J = 7.8 Hz, 2H), 7.17–7.23 (m, 8H), 7.27–7.31 (m, 3H). ^{13}C-NMR δ (ppm): 21.2, 21.3, 23.7, 30.0, 36.3, 58.2, 60.85, 60.9, 69.5, 115.1, 120.2, 125.3, 126.0, 128.7, 129.1, 129.4, 130.0, 132.7, 133.2, 137.3, 137.4, 138.7, 146.8, 150.2. Elemental analysis: $C_{30}H_{31}N_3$ required C, 83.10; H, 7.21; N, 9.69, found C, 83.37; H, 7.28; N, 9.84.

*11-Methyl-4-(3-chlorophenyl)-3-(4-methylphenyl)-7-[(4-methylphenyl)methylidene]-4,5,11-triazatricyclo[6.2.1.0*2,6*]undec-5-ene (**14l**).* Obtained from reaction of **12d** and **13b**. Reaction time 6 h, pale yellow microcrystals from ethanol, mp 196–198 °C, yield 71% (1.65 g). IR ν (cm^{-1}): 1593, 1558, 1512, 1481. ^{1}H-NMR δ (ppm): 1.89–1.96 (m, 1H), 2.09–2.24 (m, 2H), 2.34–2.42 (m, 10H), 3.50–3.59 (m, 2H), 4.37 (d, J = 5.3 Hz, 1H), 4.64 (d, J = 12.6 Hz, 1H), 6.77–6.82 (m, 2H), 7.05 (t, J = 8.1 Hz, 1H), 7.18–7.28 (m, 10H). ^{13}C-NMR δ (ppm): 21.2, 21.3, 23.7, 30.1, 36.5, 58.7, 60.9, 61.0, 69.3, 112.6, 115.4, 119.9, 125.5, 126.0, 129.1, 129.4, 129.7, 130.1, 132.8, 133.1, 134.5, 137.4, 137.6, 138.3, 147.8, 151.3. Elemental analysis: $C_{30}H_{30}ClN_3$ required C, 76.99; H, 6.46; N, 8.98, found C, 77.21; H, 6.54; N, 9.05.

*11-Methyl-4-(4-chlorophenyl)-3-(4-methylphenyl)-7-[(4-methylphenyl)methylidene]-4,5,11-triazatricyclo[6.2.1.0*2,6*]undec-5-ene (**14m**).* Obtained from reaction of **12d** and **13c**. Reaction time 12 h, pale yellow microcrystals from ethanol, mp 218–220 °C, yield 60% (1.4 g). IR ν (cm^{-1}): 1593, 1510, 1489. ^{1}H-NMR δ (ppm): 1.89–1.96 (m, 1H), 2.10–2.24 (m, 2H), 2.39–2.50 (m, 10H), 3.51 (t, J = 5.3 Hz, 1H), 3.57 (dd, J = 4.2, 12.8 Hz, 1H), 4.36 (d, J = 6.8 Hz, 1H), 4.62 (d, J = 12.8 Hz, 1H), 6.99 (d, J = 9.0 Hz, 2H), 7.12 (d, J = 9.0 Hz, 2H), 7.18–7.23 (m, 7H), 7.28 (d, J = 8.0 Hz, 2H). ^{13}C-NMR δ (ppm): 21.2, 21.3, 23.6, 30.0, 36.2, 58.3, 60.85, 60.9, 69.6, 116.3, 125.2, 126.0, 128.6, 129.2, 129.4, 130.1, 132.0, 132.9, 137.6, 137.7, 138.1, 145.2, 150.4. Elemental analysis: $C_{30}H_{30}ClN_3$ required C, 76.99; H, 6.46; N, 8.98, found C, 77.13; H, 6.53; N, 9.02.

*3,4-Bis(4-methylphenyl)-11-methyl-7-[(4-methylphenyl)methylidene]-4,5,11-triazatricyclo[6.2.1.0*2,6*]undec-5-ene (**14n**).* Obtained from reaction of **12d** and **13d**. Reaction time 4 h, pale yellow microcrystals from ethanol, mp 189–191 °C, yield 56% (1.25 g). IR ν (cm^{-1}): 1609, 1508, 1443. ^{1}H-NMR δ (ppm): 1.87–1.93 (m, 1H), 2.13–2.17 (m, 2H), 2.26 (s, 3H), 2.36–2.45 (m, 10H), 3.46 (dd, J = 4.1, 7.4 Hz, 1H), 3.55 (dd, J = 4.4, 13.0 Hz, 1H), 4.31 (d, J = 6.9 Hz, 1H), 4.63 (d, J = 13.0 Hz, 1H), 6.98–7.02 (m, 4H), 7.21–7.23 (m, 7H), 7.32 (d, J = 8.0 Hz, 2H). ^{13}C-NMR δ (ppm): 20.5, 21.2, 21.3, 23.7, 30.1, 36.5, 58.3, 60.8, 60.9, 69.9, 115.3, 124.7, 126.1, 129.1, 129.3, 129.4, 129.5, 129.9, 133.3, 133.4, 137.1, 137.3, 138.9, 144.7, 150.4. Elemental analysis: $C_{31}H_{33}N_3$ required C, 83.18; H, 7.43; N, 9.39, found C, 83.34; H, 7.50; N, 9.52.

*3-(4-Methoxyphenyl)-7-[(4-methoxyphenyl)methylidene]-11-methyl-4-phenyl-4,5,11-triazatricyclo[6.2.1.0*2,6*]undec-5-ene (**14o**).* Obtained from reaction of **12e** and **13a**. Reaction time 5 h, pale yellow microcrystals from ethanol, mp 189–191 °C, yield 51% (1.19 g). IR ν (cm^{-1}): 1597, 1508, 1497. ^{1}H-NMR δ (ppm): 1.89–1.95 (m, 1H), 2.17–2.19 (m, 2H), 2.43–2.47 (m, 4H), 3.50–3.57 (m, 2H), 3.84 (s, 3H), 3.86 (s, 3H), 4.36 (d, J = 6.2 Hz, 1H), 4.65 (d, J = 12.8 Hz, 1H), 6.86 (t, J = 7.3 Hz, 1H), 6.92–6.95 (m, 4H), 7.08 (d, J = 7.9 Hz, 2H), 7.17–7.25 (m, 5H), 7.33 (d, J = 8.6 Hz, 2H). ^{13}C-NMR δ (ppm): 23.6, 30.0, 36.4, 55.3, 58.3, 58.4, 60.8, 60.9, 69.3, 113.9, 114.7, 115.2, 120.2, 125.0, 127.3, 128.6, 128.7, 130.8, 131.8, 133.6, 146.8, 150.4, 159.0, 159.1. Elemental analysis: $C_{30}H_{31}N_3O_2$ required C, 77.39; H, 6.71; N, 9.03, found C, 77.56; H, 6.78; N, 9.25.

*4-(3-Chlorophenyl)-3-(4-methoxyphenyl)-7-[(4-methoxyphenyl)methylidene]-11-methyl-4,5,11-triazatricyclo[6.2.1.0*2,6*]undec-5-ene (**14p**).* Obtained from reaction of **12e** and **13b**. Reaction time 5 h, buff microcrystals from ethanol, mp 192–194 °C, yield 52% (1.3 g). IR ν (cm^{-1}): 1593, 1558, 1508, 1481. ^{1}H-NMR δ (ppm): 1.76–1.83 (m, 1H), 1.95–2.07 (m, 2H), 2.27–2.34 (m, 4H), 3.35 (t, J = 5.2 Hz, 1H), 3.44 (dd, J = 4.3, 12.6 Hz, 1H), 3.74 (s, 3H), 3.76 (s, 3H), 4.21 (d, J = 6.9 Hz, 1H), 4.51 (d, J = 12.6 Hz, 1H), 6.68–6.71 (m, 2H), 6.82–6.86 (m, 4H), 6.95 (t, J = 8.1 Hz, 1H), 7.09 (s, 1H), 7.11 (t, J = 2.0 Hz, 1H), 7.14 (d, J = 8.6 Hz, 2H), 7.21 (d, J = 8.6 Hz, 2H). ^{13}C-NMR δ (ppm): 23.6, 30.1, 36.6, 55.29, 55.3, 58.8, 60.8, 61.0, 69.0, 112.7, 113.9, 114.7, 115.4, 119.9, 125.0, 127.2, 128.6, 129.6, 130.8, 132.1, 133.2, 134.5, 147.9, 151.5, 159.0, 159.2. Elemental analysis: $C_{30}H_{30}ClN_3O_2$ required C, 72.06; H, 6.05; N, 8.40, found C, 72.32; H, 6.13; N, 8.57.

*4-(4-Chlorophenyl)-3-(4-methoxyphenyl)-7-[(4-methoxyphenyl)methylidene]-11-methyl-4,5,11-triazatricyclo[6.2.1.0*2,6*]undec-5-ene (**14q**).* Obtained from reaction of **12e** and **13c**. Reaction time 12 h, buff microcrystals from ethanol, mp 192–194 °C, yield 62% (1.55 g). IR ν (cm^{-1}): 1597, 1510, 1493, 1466. ^{1}H-NMR δ (ppm): 1.90–1.96 (m, 1H), 2.12–2.25 (m, 2H), 2.43–2.49 (m, 4H), 3.50–3.57 (m, 2H), 3.84 (s, 3H), 3.86 (s, 3H), 4.37 (d, J = 6.8 Hz, 1H), 4.60 (d, J = 12.6 Hz, 1H), 6.92–7.00 (m, 6H), 7.12 (d, J = 9.0 Hz, 2H), 7.21 (s, 1H), 7.23 (d, J = 8.6 Hz, 2H), 7.30 (d, J = 8.6 Hz, 2H). ^{13}C-NMR δ (ppm): 23.6, 30.1, 36.5, 55.29, 55.3, 58.5, 60.8, 60.9, 69.3, 113.9, 114.7, 116.3, 125.0, 127.2, 128.6, 130.8, 131.9, 133.2, 145.4, 151.1, 159.0, 159.3. Elemental analysis: $C_{30}H_{30}ClN_3O_2$ required C, 72.06; H, 6.05; N, 8.40, found C, 72.34; H, 6.11; N, 8.67.

*3-(4-Methoxyphenyl)-7-[(4-methoxyphenyl)methylidene]-4-(4-methylphenyl)-11-methyl-4,5,11-triazatricyclo[6.2.1.0*2,6*]undec-5-ene (**14r**).* Obtained from reaction of **12e** and **13d**. Reaction time 6 h, buff microcrystals from ethanol, mp 172–174 °C, yield 50% (1.2 g). IR ν (cm^{-1}): 1605, 1508, 1462. ^{1}H-NMR δ (ppm): 1.75–1.82 (m, 1H), 2.01–2.06 (m, 2H), 2.14 (s, 3H), 2.29–2.33 (m, 4H), 3.33–3.34 (m, 1H), 3.42 (dd, J = 4.4, 13.0 Hz, 1H), 3.73 (s, 3H), 3.75 (s, 3H), 4.20 (d, J = 6.8 Hz, 1H), 4.49 (d, J = 13.0 Hz, 1H), 6.81–6.91 (m, 8H), 7.08 (s, 1H), 7.13 (d, J = 8.6 Hz, 2H), 7.23 (d, J = 8.6 Hz, 2H). ^{13}C-NMR δ (ppm): 20.5, 23.7, 30.1, 36.5, 55.28, 55.3, 58.2, 60.8, 60.9, 69.7, 113.8, 114.6,

115.4, 124.6, 127.3, 128.8, 129.2, 129.6, 130.8, 132.2, 133.8, 144.8, 150.4, 158.9, 159.1. Elemental analysis: $C_{31}H_{33}N_3O_2$ required C, 77.63; H, 6.94; N, 8.76, found C, 77.90; H, 6.98; N, 8.94.

*11-Methyl-4-(4-methylphenyl)-3-(2-thienyl)-7-[(2-thienyl)methylidene]-4,5,11-triazatricyclo[6.2.1.0*2,6*]undec-5-ene (**14s**).* Obtained from reaction of **12f** and **13d**. Reaction time 4 h, buff microcrystals from ethanol, mp 183–185 °C, yield 51% (1.1 g). IR ν (cm^{-1}): 1612, 1508, 1447. ^{1}H-NMR δ (ppm): 1.75–1.81 (m, 1H), 2.02–2.19 (m, 2H), 2.27 (s, 3H), 2.38–2.49 (m, 4H), 3.49 (t, J = 5.4 Hz, 1H), 3.69 (dd, J = 4.3, 13.1 Hz, 1H), 4.62 (d, J = 6.9 Hz, 1H), 4.88 (d, J = 13.0 Hz, 1H), 7.01–7.11 (m, 8H), 7.29–7.35 (m, 3H). ^{13}C-NMR δ (ppm): 20.6, 23.8, 29.8, 36.5, 58.2, 60.4, 61.3, 66.4, 116.0, 117.9, 124.3, 125.2, 126.5, 127.1, 127.4, 129.3, 129.6, 130.6, 131.4, 139.0, 144.8, 145.4, 150.4. Elemental analysis: $C_{25}H_{25}N_3S_2$ required C, 69.57; H, 5.84; N, 9.74, found C, 69.81; H, 5.90; N, 9.88.

Synthesis of 4-acetyl-3-aryl-7-[(aryl)methylidene]-11-methyl-4,5,11-triazatricyclo[6.2.1.0*2,6*]undec-5-ene 16a,b (general procedure). A mixture of equimolar amounts of the appropriate 2,4-bis[(aryl)methylidene]-8-methyl-8-azabicyclo[3.2.1]octan-3-ones **12b,e** (5 mmol) and hydrazine hydrate **15** (100%) in glacial acetic acid (25 ml) was boiled under reflux for 12 hours. The reaction mixture was poured into ice-cold water (200 ml) and neutralized (sodium hydroxide, 5 N). The isolated sticky mass was triturated with ethanol (5–10 ml), and the separated solid was collected and crystallized from ethanol affording **16a,b**.

*4-Acetyl-3-(4-chlorophenyl)-7-[(4-chlorophenyl)methylidene]-11-methyl-4,5,11-triazatricyclo[6.2.1.0*2,6*]undec-5-ene (**16a**).* Obtained from reaction of **12b** and **15**. Colorless microcrystals from ethanol, mp 224–226 °C, yield 59% (1.3 g). IR ν (cm^{-1}): 1663, 1593, 1489. ^{1}H-NMR δ (ppm): 1.78–1.86 (m, 2H), 2.07–2.10 (m, 1H), 2.27–2.31 (m, 7H), 3.38–3.44 (m, 2H), 4.16 (d, J = 6.7 Hz, 1H), 4.82 (d, J = 10.3 Hz, 1H), 6.99 (s, 1H), 7.12 (d, J = 8.4 Hz, 4H), 7.25 (d, J = 8.5 Hz, 2H), 7.29 (d, J = 8.4 Hz, 2H). ^{13}C-NMR δ (ppm): 22.3, 23.6, 29.9, 36.7, 58.9, 61.3, 61.8, 63.9, 125.3, 127.3, 128.8, 129.1, 130.4, 130.6, 133.3, 133.75, 133.8, 139.9, 155.1, 170.6. Elemental analysis: $C_{24}H_{23}Cl_2N_3O$ required C, 65.46; H, 5.26; N, 9.54, found C, 65.62; H, 5.34; N, 9.70.

*4-Acetyl-3-(4-methoxyphenyl)-7-[(4-methoxyphenyl)methylidene]-11-methyl-4,5,11-triazatricyclo[6.2.1.0*2,6*]undec-5-ene (**16b**).* Obtained from reaction of **12e** and **15**. Almost colorless microcrystals from ethanol, mp 185–187 °C, yield 51% (1.1 g). IR ν (cm^{-1}): 1667, 1605, 1570, 1512. ^{1}H-NMR δ (ppm): 1.83–1.96 (m, 2H), 2.11–2.14 (m, 1H), 2.33–2.40 (m, 7H), 3.43 (dd, J = 4.4, 6.8 Hz, 1H), 3.54 (dd, J = 4.0, 10.3 Hz, 1H), 3.82 (s, 3H), 3.86 (s, 3H), 4.30 (d, J = 6.9 Hz, 1H), 4.89 (d, J = 10.3 Hz, 1H), 6.91 (d, J = 8.7 Hz, 2H), 6.94 (d, J = 8.8 Hz, 2H), 7.08 (s, 1H), 7.20–7.28 (m, 4H). ^{13}C-NMR δ (ppm): 22.4, 23.7, 30.1, 36.6, 55.29, 55.3, 58.8, 61.3, 61.7, 63.9, 113.9, 114.1, 114.3, 126.0, 127.2, 128.1, 130.8, 132.2, 133.7, 155.7, 158.9, 159.2, 170.6. Elemental analysis: $C_{26}H_{29}N_3O_3$ required C, 72.37; H, 6.77; N, 9.74, found C, 72.51; H, 6.86; N, 9.92.

Single crystal X-ray studies

Intensity data for **14a** were collected at room temperature (298 K) on an Enraf-Nonius 590 diffractometer with a Kappa CCD detector using graphite monochromated Mo-Kα (λ = 0.71073 Å) radiation.[64] Data were recorded in the rotation mode using the ϕ and ω scan technique with $2\theta_{max}$ = 33.646°. Data were corrected for absorption effects using the multi-scan method *SADABS*.[65] The structures were solved by direct methods using *SUPERFLIP*[66] implemented in the *CRYSTALS* program suit.[67] The refinement was carried out by the full-matrix least-squares method with anisotropic displacement parameters for all non-hydrogen atoms based on F^2 using *CRYSTALS*. The hydrogen atoms were positioned geometrically in their idealized positions[68] and were initially refined with soft restraints on the bond lengths and angles to regularize their geometry (C–H in the range 0.93–0.98) and U_{iso}(H) (in the range 1.2–1.5 times U_{eq} of the parent atom). Then, the positions were refined with riding constraints. The general-purpose crystallographic tool *PLATON*[69] was used for the structure analysis and presentation of the results. *ORTEP-3* for Windows[70] and *MERCURY*[71] programs were used for molecular graphics representations. Details of the data collection and refinement are given in ESI Table S13.†

In vitro antitumor screening

Tropane containing-compounds **12a–f**, **14a–s** and **16a,b** were screened for their antitumor properties against human tumor cell lines utilizing HepG2 (hepatocellular) and MCF7 (breast) carcinoma cell lines by the standard mitochondrial dependent reduction of yellow MTT [3-(4,5-dimethylthiazol-2-yl)-2,5-diphenyl-tetrazolium bromide] to purple formazan technique.[52,53] Cancer cells were obtained from the Egyptian Company for Production of Vaccines, Sera and Drugs (VACSERA), Cairo, Egypt. Media and other needs for the bio-assay were obtained from Biowest, Gibco and Lonza Companies.

Cells were suspended in RPMI-1640 medium for HepG2 and DMEM for MCF-7 in addition to 1% antibiotic–antimycotic mixture (10 000 μg ml^{-1} potassium penicillin, 10 000 μg ml^{-1} streptomycin sulfate and 25 μg ml^{-1} amphotericin B), 10% fetal bovine serum and 1% L-glutamine at 37 °C, under 5% CO_2 and 95% humidity. Cells were seeded at concentration of 10 × 10^3 cells per well in fresh complete growth medium in 96-well tissue culture microtiter plates for 24 h. Media was aspirated, fresh medium (without serum) was added and cells were incubated with different concentrations of sample to give a final concentration of (100, 50, 25, 12.5 and 6.25 μM). 0.5% DMSO was used as negative control and doxorubicin was used as positive control (standard reference). Triplicate wells were prepared for each individual dose. After 72 h of incubation, medium was aspirated, 40 μl MTT salt (2.5 mg ml^{-1}) were added to each well and incubated for further 4 h at 37 °C. To stop the reaction and dissolve the formed crystals, 200 μl of 10% sodium dodecyl sulfate (SDS) in deionized water were added to each well and incubated overnight at 37 °C. The absorbance was then measured at 595 nm and a reference wavelength of 620 nm. Data were collected as mean values for experiments performed in triplicates for each individual dose which had been measured by MTT assay. Control experiments did not exhibit significant change compared to the DMSO vehicle. The percentage of cell survival was calculated according to eqn (5).

Surviving fraction = optical density (O.D.) of treated cells/O.D. of control cells (5)

The IC_{50} (concentration required to produce 50% inhibition of cell growth compared to the control experiment) was determined using Graph-Pad PRISM version-5 software. Statistical calculations for determination of the mean and standard error values were determined by SPSS 16 software. The observed antitumor properties are presented in Table 2 (ESI Fig. S73 and S74†).

Computational chemistry

Structure optimization. The geometry of compound **14a** was optimized by the molecular mechanics force field (MM^+), followed by either semi-empirical AM1 or PM3 methods implemented in the HyperChem 8.0 package. The structures were fully optimized without constraining any parameters, thus bringing all geometric variables to their equilibrium values. The energy minimization protocol employed the Polak–Ribiere conjugated gradient algorithm.[20,72–76] Convergence to a local minimum was achieved when the energy gradient was ≤ 0.01 kcal mol^{-1}. The RHF (Restricted Hartree–Fock) method was used in the spin pairing for the two semi-empirical tools. Additionally, the molecular structure of compound **14a** in the ground state (*in vacuo*) was optimized using density functional theory (DFT). The DFT calculations were carried out with a hybrid functional B3LYP [Becke's three parameter hybrid functional using the Lee–Young–Parr (LYP) correlation functional] and 6-31G(d,p) basis set, utilizing the Gaussian 03 package.[72,74] The geometries were optimized by minimizing energies with respect to all the geometrical parameters without imposing any molecular symmetry constraints.

2D-QSAR studies. 2D-QSAR studies were undertaken utilizing comprehensive descriptors for structural and statistical analysis (CODESSA-Pro) software. Bio-active tropane containing-compounds (compounds **12a–f**, **14a–i,k–o,q–s** and **16a,b**) against MCF7 (breast) carcinoma cell line were used as a training set for constructing the QSAR model. Geometry of the training set compounds was initially optimized by AM1 technique[20,72–76] then, exported to CODESSA-Pro that includes MOPAC capability for the final geometry optimization. CODESSA-Pro calculated 711 molecular descriptors (constitutional, topological, geometrical, charge-related, semi-empirical, thermodynamical, molecular-type, atomic-type and bond-type descriptors) for the exported 25 training set antitumor active agents. Different mathematical transformations [including property, 1/property, log(property) and 1/log(property)] of the experimentally observed antitumor property/activity (IC_{50}, μM) of the training set compounds were utilized searching for the best QSAR model. The best multi-linear regression (BMLR) technique was utilized which is a stepwise search for the best *n*-parameter regression equations (where *n* stands for the number of descriptors used), based on the highest R^2 (squared correlation coefficient), R^2cvOO (squared cross-validation "leave one-out, LOO" coefficient), R^2cvMO (squared cross-validation "leave many-out, LMO" coefficient), *F* (Fisher statistical significance criteria) values, and s^2 (standard deviation). The QSAR models up to 5-descriptor model describing the bio-activity of the antitumor tropane-containing active agents were generated (obeying the thumb rule of 5 : 1, which is the ratio between the data points and the number of QSAR descriptor).

In order to attain appropriate validation of the QSAR study, part of the available data set was utilized for building the model and the remaining data points were used for external validation.[60,61]

(1) All the available data points (25 tropane containing-compounds exhibiting antitumor properties against MCF7 cell line, **12a–f**, **14a–i,k–o,q–s** and **16a,b**) were arranged in the descending order of IC_{50} values and separated into three subsets (*A*, *B* and *C*) by selection of every third point from the original dataset in order to obtain a similar distribution of the investigated property values for each subset.

(2) Three new datasets were constructed using the three binary sums combinations: *A* + *B*, *A* + *C*, and *B* + *C*. Then, BMLR-QSAR modeling procedure was applied to the three datasets obtained.

(3) The complementary parts to each of the three datasets (*C*, *B* and *A*, respectively) were used as external validation datasets by considering their consistency.

The observed BMLR-QSAR models as well as the estimated activity values are exhibited in ESI Tables S4–S12 and Fig. S75–S77.†

Acknowledgements

The authors are grateful for Global Napi Pharmaceuticals (Dr Peter Mehany, Chairman and Managing Director and Dr Salwa Gamil, Research and Development Director) for facilities allowed.

Notes and references

1 W. J. Griffin and G. D. Lin, *Phytochemistry*, 2000, **53**, 623–637.
2 M. Reina, E. Burgueño-Tapia, M. A. Bucio and P. Joseph-Nathan, *Phytochemistry*, 2010, **71**, 810–815.
3 X. R. Wang, M. Chen, C. X. Yang, X. Q. Liu, L. Zhang, X. Z. Lan, K. X. Tang and Z. H. Liao, *Physiol. Plant.*, 2011, **143**, 309–315.
4 W. Qiang, K. Xia, Q. Zhang, J. Zeng, Y. Huang, C. Yang, M. Chen, X. Liu, X. Lan and Z. Liao, *Phytochemistry*, 2016, **127**, 12–22.
5 B. Dräger, *Phytochemistry*, 2006, **67**, 327–337.
6 L. Zhu, L.-M. Yang, Y.-Y. Cui, P.-L. Zheng, Y.-Y. Niu, H. Wang, Y. Lu, Q.-S. Ren, P.-J. Wei and H.-Z. Chen, *Acta Pharmacol. Sin.*, 2008, **29**, 177–184.
7 M. Purushotham, A. Sheri, D.-P. Pham-Huu, B. K. Madras, A. Janowsky and P. C. Meltzer, *Bioorg. Med. Chem. Lett.*, 2011, **21**, 48–51.
8 D.-P. Pham-Huu, J. R. Deschamps, S. Liu, B. K. Madras and P. C. Meltzer, *Bioorg. Med. Chem.*, 2007, **15**, 1067–1082.
9 S. S. Kulkarni, T. A. Kopajtic, J. L. Katzb and A. H. Newman, *Bioorg. Med. Chem.*, 2006, **14**, 3625–3634.

10 M. Mishra, R. Kolhatkar, J. Zhen, I. Parrington, M. E. A. Reithb and A. K. Dutta, *Bioorg. Med. Chem.*, 2008, **16**, 2769–2778.

11 C. Jin, H. A. Navarro and F. Ivy Carroll, *Bioorg. Med. Chem.*, 2009, **17**, 5126–5132.

12 C. Jin, H. A. Navarro and F. Ivy Carroll, *Bioorg. Med. Chem.*, 2008, **16**, 5529–5535.

13 C. Jin, H. A. Navarro, K. Page and F. Ivy Carroll, *Bioorg. Med. Chem.*, 2008, **16**, 6682–6688.

14 S. Zhang, S. Izenwasser, D. Wade, L. Xu and M. L. Trudell, *Bioorg. Med. Chem.*, 2006, **14**, 7943–7952.

15 J. Bussenius, C. M. Blazey, N. Aay, N. K. Anand, A. Arcalas, T. Baik, O. J. Bowles, C. A. Buhr, S. Costanzo, J. K. Curtis, S. C. DeFina, L. Dubenko, T. S. Heuer, P. Huang, C. Jaeger, A. Joshi, A. R. Kennedy, A. I. Kim, K. Lara, J. Lee, J. Li, J. C. Lougheed, S. Ma, S. Malek, J.-C. L. Manalo, J.-F. Martini, G. McGrath, M. Nicoll, J. M. Nuss, M. Pack, C. J. Peto, T. H. Tsang, L. Wang, S. W. Womble, M. Yakes, W. Zhang and K. D. Rice, *Bioorg. Med. Chem. Lett.*, 2012, **22**, 5396–5404.

16 M. J. Di Grandi, D. M. Berger, D. W. Hopper, C. Zhang, M. Dutia, A. L. Dunnick, N. Torres, J. I. Levin, G. Diamantidis, C. W. Zapf, J. D. Bloom, Y.-B. Hu, D. Powell, D. Wojciechowicz, K. Collins and E. Frommer, *Bioorg. Med. Chem. Lett.*, 2009, **19**, 6957–6961.

17 S. M. Wilhelm, L. Adnane, P. Newell, A. Villanueva, J. M. Llovet and M. Lynch, *Mol. Cancer Ther.*, 2008, **7**, 3129–3140.

18 J. A. McCubrey, M. Milell, A. Tafuri, A. M. Martelli, P. Lunghi, A. Bonati, M. Cervello, J. T. Lee and L. S. Steelman, *Curr. Opin. Invest. Drugs*, 2008, **9**, 614–630.

19 R. F. George, S. S. Panda, E. M. Shalaby, A. M. Srour, I. S. Ahmed Farag and A. S. Girgis, *RSC Adv.*, 2016, **6**, 45434–45451.

20 A. S. Girgis, A. F. Mabied, J. Stawinski, L. Hegazy, R. F. George, H. Farag, E. M. Shalaby and I. S. Ahmed Farag, *New J. Chem.*, 2015, **39**, 8017–8027.

21 A. S. Girgis, S. S. Panda, A. M. Srour, H. Farag, N. S. M. Ismail, M. Elgendy, A. K. Abdel-Aziz and A. R. Katritzky, *Org. Biomol. Chem.*, 2015, **13**, 6619–6633.

22 A. S. Girgis, S. S. Panda, M. N. Aziz, P. J. Steel, C. D. Hall and A. R. Katritzky, *RSC Adv.*, 2015, **5**, 28554–28569.

23 A. S. Girgis, S. S. Panda, E. M. Shalaby, A. F. Mabied, P. J. Steel, C. D. Hall and A. R. Katritzky, *RSC Adv.*, 2015, **5**, 14780–14787.

24 A. S. Girgis, S. S. Panda, I. S. Ahmed Farag, A. M. El-Shabiny, A. M. Moustafa, N. S. M. Ismail, G. G. Pillai, C. S. Panda, C. D. Hall and A. R. Katritzky, *Org. Biomol. Chem.*, 2015, **13**, 1741–1753.

25 R. F. George, N. S. M. Ismail, J. Stawinski and A. S. Girgis, *Eur. J. Med. Chem.*, 2013, **68**, 339–351.

26 A. S. Girgis, J. Stawinski, N. S. M. Ismail and H. Farag, *Eur. J. Med. Chem.*, 2012, **47**, 312–322.

27 A. R. Katritzky, A. S. Girgis, S. Slavov, S. R. Tala and I. Stoyanova-Slavova, *Eur. J. Med. Chem.*, 2010, **45**, 5183–5199.

28 A. S. Girgis, *Eur. J. Med. Chem.*, 2009, **44**, 1257–1264.

29 A. S. Girgis, *Eur. J. Med. Chem.*, 2009, **44**, 91–100.

30 A. S. Girgis, H. M. Hosni and F. F. Barsoum, *Bioorg. Med. Chem.*, 2006, **14**, 4466–4476.

31 H. I. El-Subbagh, S. M. Abu-Zaid, M. A. Mahran, F. A. Badria and A. M. Al-Obaid, *J. Med. Chem.*, 2000, **43**, 2915–2921.

32 S. A. F. Rostom, G. S. Hassan and H. I. El-Subbagh, *Arch. Pharm.*, 2009, **342**, 584–590.

33 P. Ambure and K. Roy, *RSC Adv.*, 2016, **6**, 28171–28186.

34 K. Roy, S. Kar and P. Ambure, *Chemom. Intell. Lab. Syst.*, 2015, **145**, 22–29.

35 A. S. Girgis, F. H. Osman, F. A. El-Samahy and I. S. Ahmed-Farag, *Chem. Pap.*, 2006, **60**, 237–242.

36 F. F. Barsoum, H. M. Hosni and A. S. Girgis, *Bioorg. Med. Chem.*, 2006, **14**, 3929–3937.

37 S. Fatma, D. Singh, P. Ankit, P. Mishra, M. Singh and J. Singh, *Tetrahedron Lett.*, 2014, **55**, 2201–2207.

38 S. Fatma, P. K. Singh, P. Ankit, Shireen, M. Singh and J. Singh, *Tetrahedron Lett.*, 2013, **54**, 6732–6736.

39 J. Liu, M. Lei and L. Hu, *Green Chem.*, 2012, **14**, 840–846.

40 F. Chen, M. Lei and L. Hu, *Tetrahedron*, 2013, **69**, 2954–2960.

41 Y. Chen, W. Shan, M. Lei and L. Hu, *Tetrahedron Lett.*, 2012, **53**, 5923–5925.

42 H. Schenk and P. Benci, *Acta Crystallogr., Sect. B: Struct. Crystallogr. Cryst. Chem.*, 1972, **28**, 538–543.

43 M. Laing, N. Sparrow and P. Sommerville, *Acta Crystallogr., Sect. B: Struct. Crystallogr. Cryst. Chem.*, 1975, **31**, 2848–2851.

44 J. Vilches, F. Florencio and S. García-Blanco, *Acta Crystallogr., Sect. B: Struct. Crystallogr. Cryst. Chem.*, 1981, **37**, 361–364.

45 J. Bode and C. H. Stam, *Acta Crystallogr., Sect. B: Struct. Crystallogr. Cryst. Chem.*, 1982, **38**, 333–335.

46 B. Krebs and U. Flörke, *Acta Crystallogr., Sect. C: Cryst. Struct. Commun.*, 2004, **60**, o118–o119.

47 M. R. Wood, T. A. Brettell, H. W. Thompson and R. A. Lalancette, *Acta Crystallogr., Sect. E: Struct. Rep. Online*, 2008, **64**, o525.

48 Z.-P. Chen, S.-P. Wang, X.-M. Li, J. Tang and J.-G. Lin, *Acta Crystallogr., Sect. E: Struct. Rep. Online*, 2008, **64**, o1732.

49 L.-M. Yang, L. Zhu, Y.-Y. Niu, H.-Z. Chen and Y. Lu, *Acta Crystallogr., Sect. E: Struct. Rep. Online*, 2008, **64**, o2331.

50 L.-M. Yang, Y.-F. Xie, Y.-F. Gu, H.-Z. Chen and Y. Lu, *Acta Crystallogr., Sect. E: Struct. Rep. Online*, 2009, **65**, o1037.

51 M. R. Wood, H. W. Thompson, T. A. Brettell and R. A. Lalancette, *Acta Crystallogr., Sect. C: Cryst. Struct. Commun.*, 2010, **66**, m4–m8.

52 B. S. El-Menshawi, W. Fayad, K. Mahmoud, S. M. El-Hallouty, M. El-Manawaty, M. H. Olofsson and S. Linder, *Indian J. Exp. Biol.*, 2010, **48**, 258–264.

53 M. I. Thabrew, R. D. Hughes and I. G. McFarlane, *J. Pharm. Pharmacol.*, 1997, **49**, 1132–1135.

54 X. Zhao, Y. Wang, J.-J. Gao and J.-J. Yin, *Asian Pac. J. Trop. Med.*, 2014, **7**, 468–472.

55 *CODESSA-Pro manual*, pp. 54, 61, 62, 73.

56 S. S. Panda, O. S. Detistov, A. S. Girgis, P. P. Mohapatra, A. Samir and A. R. Katritzky, *Bioorg. Med. Chem. Lett.*, 2016, **26**, 2198–2205.

57 R. N. Naumov, S. S. Panda, A. S. Girgis, R. F. George, M. Farhat and A. R. Katritzky, *Bioorg. Med. Chem. Lett.*, 2015, **25**, 2314–2320.
58 M. A. Ibrahim, S. S. Panda, A. A. Oliferenko, P. V. Oliferenko, A. S. Girgis, M. Elagawany, F. Z. Küçükbay, C. S. Panda, G. G. Pillai, A. Samir, K. Tämm, C. D. Hall and A. R. Katritzky, *Org. Biomol. Chem.*, 2015, **13**, 9492–9503.
59 S. S. Panda, S. Liaqat, A. S. Girgis, A. Samir, C. D. Hall and A. R. Katritzky, *Bioorg. Med. Chem. Lett.*, 2015, **25**, 3816–3821.
60 A. R. Katritzky, S. H. Slavov, D. A. Dobchev and M. Karelson, *Bioorg. Med. Chem.*, 2008, **16**, 7055–7069.
61 A. R. Katritzky, L. M. Pacureanu, S. Slavov, D. A. Dobchev and M. Karelson, *Bioorg. Med. Chem.*, 2006, **14**, 7490–7500.
62 H. N. Pati, U. Das, S. Das, B. Bandy, E. De Clercq, J. Balzarini, M. Kawase, H. Sakagami, J. W. Quail, J. P. Stables and J. R. Dimmock, *Eur. J. Med. Chem.*, 2009, **44**, 54–62.
63 A. F. Mabied, A. S. Girgis, E. M. Shalaby, R. F. George, B. E. M. El-Gendy and F. N. Baselious, *J. Heterocycl. Chem.*, 2016, **53**, 1074–1080.
64 R. W. W. Hooft, *Collect: Data Collection Software*, Nonius BV, Delft, Netherlands, 1998.
65 G. M. Sheldrick, *Bruker. SADABS (Version 2014/4)*, Bruker AXS Inc., Madison, Wisconsin, USA.
66 L. Palatinus and G. Chapuis, *J. Appl. Crystallogr.*, 2007, **40**, 786–790.
67 P. W. Betteridge, J. R. Carruthers, R. I. Cooper, K. Prout and D. J. Watkin, *J. Appl. Crystallogr.*, 2003, **36**, 1487.
68 R. I. Cooper, A. L. Thompson and D. J. Watkin, *J. Appl. Crystallogr.*, 2010, **43**, 1100–1107.
69 A. L. Spek, *Acta Crystallogr., Sect. D: Biol. Crystallogr.*, 2009, **65**, 148–155.
70 L. J. Farrugia, *J. Appl. Crystallogr.*, 2012, **45**, 849–854.
71 C. F. Macrae, I. J. Bruno, J. A. Chisholm, P. R. Edgington, P. McCabe, E. Pidcock, L. Rodriguez-Monge, R. Taylor, J. van de Streek and P. A. Wood, *J. Appl. Crystallogr.*, 2008, **41**, 466–470.
72 A. S. Girgis, M. N. Aziz, E. M. Shalaby, D. O. Saleh, F. M. Asaad, W. I. El-Eraky and I. S. Ahmed Farag, *J. Chem. Crystallogr.*, 2016, **46**, 280–289.
73 H. M. Faidallah, S. S. Panda, J. C. Serrano, A. S. Girgis, K. A. Khan, K. A. Alamry, T. Therathanakorn, M. J. Meyers, F. M. Sverdrup, C. S. Eikhoff, S. G. Getchell and A. R. Katritzky, *Bioorg. Med. Chem.*, 2016, **24**, 3527–3539.
74 A. S. Girgis, M. N. Aziz, E. M. Shalaby, D. O. Saleh, N. Mishriky, W. I. El-Eraky and I. S. Ahmed Farag, *Z. Kristallogr. - Cryst. Mater.*, 2016, **231**, 179–187.
75 E. M. Shalaby, A. S. Girgis, A. M. Moustafa, A. M. ElShaabiny, B. E. M. El-Gendy, A. F. Mabied and I. S. Ahmed Farag, *J. Mol. Struct.*, 2014, **1075**, 327–334.
76 A. S. Girgis, H. Farag, N. S. M. Ismail and R. F. George, *Eur. J. Med. Chem.*, 2011, **46**, 4964–4969.